

RESEARCH ARTICLE



A new approach on the stability and convergence of a time-space nonuniform finite difference approximation of a degenerate Kawarada problem

Eduardo Servin Torres and Qin Sheng (1)

Department of Mathematics and Center for Astrophysics, Space Physics, and Engineering Research, Baylor University, Waco, TX, USA

ABSTRACT

Nonlinear Kawarada equations have been used to model solid fuel combustion processes in the oil industry. An effective way to approximate solutions of such equations is to take advantage of the finite difference configurations. Traditionally, the nonlinear term of the equation is linearized while the numerical stability of a difference scheme is investigated. This leaves certain ambiguity and uncertainty in the analysis. Based on nonuniform grids generated through a quenching-seeking moving mesh method in space and adaptation in time, this paper introduces a completely new stability analysis of the approximation without freezing the nonlinearity involved. Pointwise orders of convergence are investigated numerically. Simulation experiments are carried out to accompany the mathematical analysis to strengthen our conclusions.

ARTICLE HISTORY

Received 20 October 2023 Revised 7 February 2024 Accepted 8 April 2024

KEYWORDS

Kawarada problem; quenching solution; finite difference method; nonuniform meshes; convergence; stability

MATHEMATICS SUBJECT CLASSIFICATIONS

0M25; 65C30; 65M12; 65M22; 65N12

1. Introduction

This paper focuses on the study of a mathematical model for a quenching process, which interprets temperature profiles of solid fuel combustion. The best way to think about the process is to be inside a combustion chamber. In the beginning, there is a set of fuels with low temperatures within the chamber. But as the fuel temperature begins to reach a certain critical point, an explosion of fuel occurs. Nonlinear Kawarada equations have been used in the phenomena [9,13]. To optimize a combustion process, solutions of Kawarada equations must be found accurately until the explosion which is defined as the quench of the solutions [5,14]. An indication of quenching is the blow-up of the nonlinear source terms of the Kawarada equations [16]. The time at such a blow-up and its corresponding peak chamber temperature are referred to as the critical time and critical temperature, respectively [5,16]. The location of the peak temperature is called the *quenching location* [2,14]. It has been known that the supremum of the temporal derivative of the temperature field function, that is, the solution of a Kawarada equation, tends to be unbounded. These have introduced a tremendous number of challenges to the analysis and approximation of the Kawarada solutions. Based on our investigations with uniform meshes [21], in this paper, we provide an alternative stability analysis without freezing any nonlinear terms of the one-dimensional Kawarada equation while the accuracy of the computations is improved due to applications of variable time-space grids.

For the sake of simplicity in derivations, we focus on a typical one-dimensional quenching model problem in this paper. In this circumstance, the idealized solid fuel combustion dynamics can be

characterized through the following degenerate initial-boundary value problem [2,18,19].

$$d(x)\frac{\partial q}{\partial t} = \frac{\partial^2 q}{\partial x^2} + \phi(q), \quad 0 < x < a, \ 0 \le t_0 < t \le T_a, \ a > 0, \tag{1}$$

$$q(0,t) = q(a,t) = 0, \quad t > t_0,$$
 (2)

$$q(x, t_0) = q_0(x), \quad 0 \le x \le a,$$
 (3)

where T_a is the quenching time solely depending on a [13,16]. We adopt the following Bernoulli type degenerate function and a nonlinear reaction function,

$$d(x) = \alpha x^{\theta} (a - x)^{1 - \theta}, \quad \phi(q) = (b - q)^{-r}, \quad \alpha > 0, \ b > 0, \ r > 0,$$
(4)

where $0 \le \theta \le 1$ is determined stochastically. For simplicity, we set b = 1 and let $N \in \mathbb{N}^+$, $N \gg 1$. For $s_0 = 0$, $s_{N+1} = 1$, we define an arbitrary mesh domain $\mathcal{E}_N = \{s_1, s_2, \ldots, s_N\}$ in which $s_k = s_{k-1} + h_{k-1}$, $k = 1, \ldots, N+1$, where $0 < h_k \ll 1$ are variable space step sizes utilized with $\sum_{k=0}^{N} h_k = 1$. It follows that $\bar{\mathcal{E}}_N = \{s_0, s_1, \ldots, s_N, s_{N+1}\}$. Denote $q_k = q_k(t)$ as an approximation of $q(s_k, t)$, $k = 0, 1, \ldots, N+1$.

The structure of this paper is the following. A solution approximation utilizing the Crank-Nicholson method will be derived in Section 2. We shall then introduce a new way of stability analysis. Section 3 will be used to explore the convergence of the solution sequence and its differences through intensive analysis. Numerical experiments that highlight the characteristics of the approximations, such as the computed orders of convergence, will be presented in Section 4. Section 5 will be devoted to conclusions and expectations that highlight the most important information and results. Matrix spectral norm will be employed throughout the paper unless otherwise declared.

2. Nonuniform finite difference approximation and stability

Consider the transformation x/a = s. Thus, problem (1)–(4) can be converted to

$$d(s)\frac{\partial q}{\partial t} = \frac{1}{a^2}\frac{\partial^2 q}{\partial s^2} + \phi(q), \quad 0 < s < 1, \ 0 \le t_0 < t \le T_a, \ a > 0, \tag{5}$$

$$q(0,t) = q(1,t) = 0, \quad t > t_0,$$
 (6)

$$q(s,t_0) = q_0(s), \quad 0 \le s \le 1,$$
 (7)

$$d(s) = a\alpha s^{\theta} (1-s)^{1-\theta}, \quad \phi(q) = (b-q)^{-r}.$$
 (8)

Denote $h = h_{\text{max}} = \max_{0 \le k \le N} h_k$ and $h_{\text{min}} = \min_{0 \le k \le N} h_k$, $0 \le k \le N$. We consider following nonuniform central difference approximation for the second derivative [1,11], that is,

$$\frac{\partial^2 q}{\partial s^2}(s_k, t) = \frac{2}{h_{k-1}(h_k + h_{k-1})} q_{k-1} - \frac{2}{h_{k-1}h_k} q_k + \frac{2}{h_k(h_k + h_{k-1})} q_{k+1} + \mathcal{O}(h), \quad s_k \in \mathcal{E}_N.$$

Dropping the truncation error, we acquire the following semidiscretized system following (5)–(7),

$$\frac{dq}{dt}(t) = Pq(t) + \psi(q), \quad t_0 < t < T_a, \tag{9}$$

$$q(t_0) = q_0, (10)$$

72.

where $q = (q_1, q_2, ..., q_N)^{\top}$, $\psi(q) = (\psi_1, \psi_2, ..., \psi_N)^{\top} \in \mathbb{R}^N$ with $\psi_k = \phi(q_k)/d_k$, k = 1, 2, ..., N, $d_k = a\alpha s_k^{\theta} (1 - s_k)^{1-\theta}$, $P = BT \in \mathbb{R}^{N \times N}$ for which $B = \text{diag}[1/d_1, 1/d_2, ..., 1/d_N]$ and

$$T = \frac{2}{a^2} \begin{bmatrix} -\frac{1}{h_1 h_0} & \frac{1}{h_1 (h_0 + h_1)} \\ \frac{1}{h_1 (h_1 + h_2)} & -\frac{1}{h_2 h_1} & \frac{1}{h_2 (h_1 + h_2)} \\ & & & \vdots \\ \frac{1}{h_{N-2} (h_{N-2} + h_{N-1})} \end{bmatrix}$$

$$\frac{1}{h_{N-1}h_{N-2}} \frac{1}{h_{N-1}(h_{N-2}+h_{N-1})} = \frac{1}{h_{N-1}(h_{N-2}+h_{N-1})} = \frac{1}{h_{N}h_{N-1}}$$

We further denote

$$\psi_{\min} = \min_{k=1,2,...,N} \psi_k, \, \psi_{\max} = \max_{k=1,2,...,N} \psi_k. \tag{11}$$

Note that solutions of (9), (10) exist and are unique if $Pq + \psi$ satisfies the Lipschitz condition [12]. Its solution can be approximated via various existing numerical methods such as Runge-Kutta algorithms or integral configurations [4,8,15]. However, we may notice that the formal solution to the initial value problem can be formulated as

$$q(t) = E(tP)q_0 + \int_{t_0}^t E((t - \xi)P)\psi(q(\xi)) \,d\xi, \quad t \ge t_0,$$
(12)

where $E(\cdot) = \exp(\cdot) \in \mathbb{R}^{N \times N}$ is a matrix exponential. An application of the trapezoidal rule for (12) yields a second-order approximation, that is,

$$q(t) = E(\tau P)q_0 + \frac{\tau}{2} \left[\psi(q(t)) + E(\tau P)\psi(q_0) \right] + \mathcal{O}(\tau^2),$$

where $\tau = t - t_0$, $0 < \tau_i \ll 1$, serving as a realistic time step. The matrix exponential E can be approximated effectively via an appropriate formula, such as the P-acceptable [1/1] Padé approximant [6,12],

$$E(\tau P) = \left(I - \frac{\tau}{2}P\right)^{-1} \left(I + \frac{\tau}{2}P\right) + \mathcal{O}(\tau^3), \quad 0 < \tau \ll 1.$$
(13)

The above approximation leads to a Crank-Nicolson type scheme. Set $t_{\ell} = t_0 + \ell \tau_i, \ \ell = 0, 1, \dots$ Utilizing (13), we arrive at the nonlinear system

$$q^{(j+1)} = \left(I - \frac{\tau_j}{2}P\right)^{-1} \left(I + \frac{\tau_j}{2}P\right) \left[q^{(j)} + \frac{\tau_j}{2}\psi\left(q^{(j)}\right)\right] + \frac{\tau_j}{2}\psi\left(q^{(j+1)}\right), \quad j = 0, 1, \dots,$$
 (14)

$$q^{(0)} = q_0. (15)$$

Note that the time step used in (14) can be flexible or based on a particular adaptation method, given that proper Courant constraints are satisfied [21]. This enables the potential for temporal adaptation [6,20]. In fact, we may expect that $\tau_{j+1} \leq \tau_j$, $\forall j$, due to the anticipated quenching singularity.

To discuss the stability of (14)–(15), we must first verify that $\left\|\left(I - \frac{\tau_j}{2}P\right)^{-1}\left(I + \frac{\tau_j}{2}P\right)\right\| \le 1$ for the matrix P introduced by (9). If the above inequality is true then it will make the analysis relatively straightforward later on. The following definitions and lemmas will build a basis for this purpose. Let $O \in \mathbb{R}^{N \times N}$ be a zero matrix.

Definition 2.1 ([7]): Let $Q \in \mathbb{R}^{N \times N}$ be symmetric. We say that Q is positive definite, Q > O, if and only if $x^{\mathsf{T}}Qx > 0$ for all $x \in \mathbb{R}^N$. In addition if a symmetric matrix $P \geq O$ then it is semi-positive definite. Furthermore, let $R \in \mathbb{R}^{N \times N}$ also be symmetric. We say that Q > R if and only if Q - R is positive definite.

Lemma 2.2: Let $Q_1, Q_2 \in \mathbb{R}^{N \times N}$ be symmetric and $R \in \mathbb{R}^{N \times N}$. Then $Q_1 \leq Q_2$ implies $RQ_1R^{\mathsf{T}} \leq RQ_2R^{\mathsf{T}}$.

Proof: Suppose $Q_1 \leq Q_2$. By definition then $x^{\mathsf{T}}(Q_1 - Q_2)x \leq 0 \quad \forall \ x \in \mathbb{R}^N$. Let $R \in \mathbb{R}^{N \times N}$. Notice for the matrix $R(Q_1 - Q_2)R^{\mathsf{T}}$ there is

$$x^{\mathsf{T}}R(Q_1 - Q_2)R^{\mathsf{T}}x = y^{\mathsf{T}}(Q_1 - Q_2)y \le 0.$$

Hence
$$R(Q_1 - Q_2)R^{\mathsf{T}} \leq O$$
 and $RQ_1R^{\mathsf{T}} \leq RQ_2R^{\mathsf{T}}$.

Lemma 2.3: Let $Q \in \mathbb{R}^{n \times n}$ be positive definite, that is, Q > O and Q is symmetric, and let $c \in \mathbb{R}^+$ be a constant. Then $||Q|| \le c$ is equivalent to $Q \le cI$.

Proof: Assume that Q > O, $Q \le cI$. This results in

$$O \le cI - Q$$
.

Let $\lambda_{cI-Q} > 0$ be an eigenvalue of cI-Q and x be the corresponding eigenvector. Therefore

$$(cI - Q)x = \lambda_{cI-Q}x.$$

The above is equivalent to

The decite to equivalent

$$(cI - Q - \lambda_{cI-Q}I)x = -(Q - (c - \lambda_{cI-Q})I)x = 0$$
$$Qx = (c - \lambda_{cI-Q})x.$$

Thus $c - \lambda_{cI-Q}$ is an eigenvalue of Q. Recall that $\lambda_{cI-Q} > 0$ therefore $\lambda_Q = c - \lambda_{cI-Q} \le c$. Since Q is symmetric it follows immediately that

$$0<\|Q\|=\rho(Q)\leq c.$$

 Notice that the discussion works in a reversed way too, based on the definition of the matrix spectral norm. Therefore the proof is completed.

One strategy to show $\left(I - \frac{\tau_j}{2}P\right)^{-1} \left(I + \frac{\tau_j}{2}P\right) \leq I$ seems to be achievable through Lemma 2.3. However, challenges exist since the matrix product involved is non-symmetric due to the fact that P is non-symmetric in general. Therefore, instead, let us switch our attention to

$$Q = \left(I - \frac{\tau_j}{2}P\right)^{-1} \left(I + \frac{\tau_j}{2}P\right) \left(I + \frac{\tau_j}{2}P^{\mathsf{T}}\right) \left(I - \frac{\tau_j}{2}P^{\mathsf{T}}\right)^{-1}.$$
 (16)

Notice *Q* is symmetric and all that is needed to apply Lemma 2.3, is to prove *Q* is positive definite. We shall need the following definitions from fundamental matrix theory.

Definition 2.4 ([3,17]): A Z-matrix $Z \in \mathbb{R}^{N \times N}$ is a matrix with $z_{ii} \leq 0, \ \forall \ i \neq j$.

Definition 2.5 ([3,17]): An M-matrix is a Z-matrix with the real parts of all its eigenvalues being non-negative.

Lemma 2.6: A matrix $W \in \mathbb{R}^{N \times N}$ is an M-matrix if and only if it can be expressed as W = sI - Cwhere $C \in \mathbb{R}^{N \times N}$ is a matrix with $c_{ij} \geq 0$, $1 \leq i, j \leq N$, and s is a constant with $s > \rho(C)$. $\rho(C)$ is the largest absolute eigenvalue of matrix C.

Proof: First the converse direction. Suppose the matrix W is a matrix that can be written as W = sI - C where $c_{ij} \ge 0$, $\forall i, j$, and $s > \rho(C)$. Since $c_{ij} \ge 0 \ \forall i, j$ then $-c_{ij} \le 0$, $\forall i, j$. Therefore $w_{ii} \leq 0, \ \forall i \neq j \text{ and } W \text{ is a } Z\text{-matrix. Now using properties of eigenvalues. } \lambda_i(W) = \lambda_i(sI - C) = 0$ $s - \lambda_i(C)$. Since $s > \rho(C)$ then $s > \text{Re}(\lambda_i(C))$ for any eigenvalues. So $\text{Re}(\lambda_i(W)) > 0$. Thus all eigenvalues of W have non-negative real parts.

Now, in the forward direction, suppose the matrix W is a Z-Matrix with real parts of all its eigenvalues being non-negative. Let C = -(W - sI) where $s \in \mathbb{R}$. Since W is a Z-matrix, we have $w_{ii} < -\infty$ $0 \ \forall \ i \neq j \ \text{and} \ c_{ii} \geq 0 \ \forall \ i \neq j$. In order to make the diagonal positive we force $s > \max |w_{ii}|$. Now, we notice by eigenvalue properties $\lambda_i(W) = \lambda_i(sI - C) = s - \lambda_i(C)$. By the Perron-Frobenius theorem [10], C must have a positive eigenvalue with $\lambda_i(C) = \rho(C)$. Hence $s - \rho(C)$ is also an eigenvalue of W. Therefore $Re(\lambda_i(W)) = s - Re(\lambda_i(C)) \ge s - \rho(C) > 0$. This completes our proof.

Lemma 2.7: All M-matrices are monotone and inverse positive.

Proof: Let D be a general M-matrix. By definition then D = sI - B where $s > \rho(B)$ and $b_{ij} \ge 0 \,\forall \, 0 \le B$ $i,j \le n$. Note $\rho(\frac{1}{s}B) = \frac{1}{s}\rho(B) < 1$. Therefore the series $\sum_{n=1}^{\infty} \frac{1}{s^n} B^n$ must converge. This leads to the following property.

$$D^{-1} = (sI - B)^{-1} = \frac{1}{s} \left(I - \frac{1}{s} B \right)^{-1} = \frac{1}{s} \sum_{n=0}^{\infty} \frac{1}{s^n} B^n.$$

Hence D^{-1} is an infinite series of matrices whose entries are positive so the entries of D^{-1} are positive as a result. This means that every M-matrix has an inverse whose entries are positive. All there is left to show is that every M-matrix is monotone. For a matrix to be monotone it means for all real vectors v, Av > 0 implies v > 0. Suppose that Dx > 0, for a general M-matrix, D. Recall since D is a M-matrix then D^{-1} has positive entries. Notice

$$Dv \ge 0,$$

$$D^{-1}Dv = v \ge 0.$$

This only works because D^{-1} has positive entries and is being multiplied by a vector, $D\nu$ which also has positive entries.

We need the following Gershgorin Circle Criterion.

Lemma 2.8 ([12,21]): Let $B \in \mathbb{C}^{d \times d}$ be an arbitrary irreducible matrix where $d \in \mathbb{Z}^+$. Then

$$\sigma(B) \subset \cup_{i=1}^d \mathbb{S}_i$$

where

205 206

207

208 209

210

211

212 213

214

215

216

217

218

219

220

221

222

223

224

225 226

227

228

229

234

235

236

237

238

239 240

241

242 243

244

245 246

247

248 249

250

251 252 253

254

255

$$\mathbb{S}_i = \left\{ z \in \mathbb{C} : |x - b_{i,i}| \le \sum_{j=1, i \ne j}^d |b_{i,j}| \right\}$$

and $\sigma(B)$ is the set containing all eigenvalues of B. Moreover, $\lambda \in \sigma(B)$ may lie on $\partial \mathbb{S}_{i^0}$ for some $i^0 \in \mathcal{S}_{i^0}$ $\{1, 2, \ldots, d\}$ only if $\lambda \in \partial \mathbb{S}_i$ for all $i \in \{1, 2, \ldots, d\}$. \mathbb{S}_i are known as Gershgorin discs.

Being prepared with the definitions and lemmas, we may now proceed with Q defined in (16).

Lemma 2.9: Eigenvalues of the matrix $P + P^{\mathsf{T}}$ are non-positive.

Proof: The proof is straightforward. Note that the matrix is symmetric so its eigenvalues are real. By the Gershgorin Circle Criterion, the real part of any eigenvalue of P is non-positive. Therefore the real part of any eigenvalue of -P is non-negative. Notice the structure of the matrix -P, that is,

$$-P = \frac{2}{a^2} \begin{bmatrix} \frac{1}{h_1 h_0 d_1} & \frac{-1}{h_1 (h_0 + h_1) d_1} \\ \frac{1}{h_1 (h_1 + h_2) d_2} & \frac{1}{h_2 h_1 d_2} & \frac{-1}{h_2 (h_1 + h_2) d_2} \\ & \cdots & \frac{-1}{h_{n-2} (h_{n-2} + h_{n-1}) d_{n-1}} \end{bmatrix}$$

$$\frac{\frac{1}{h_{n-1}h_{n-2}d_{n-1}}}{\frac{1}{h_{n-1}(h_{n-1}+h_n)d_n}} \frac{-1}{h_{n-1}(h_{n-2}+h_{n-1})d_{n-1}} \frac{1}{h_nh_{n-1}d_n}$$

Therefore by Definition 2.5, -P, $-P^{\mathsf{T}}$ must be M-matrices. Therefore -P = sI - C where $c_{ij} \ge 0$, $\forall i,j$ and $s \ge \rho(C)$. Similarly, $-P^{\mathsf{T}} = sI - C^{\mathsf{T}}$. A combination yields $-P - P^{\mathsf{T}} = 2sI - (C + C^{\mathsf{T}})$. So $-P - P^{\mathsf{T}}$ must be an M-matrix. Finally according to Lemma 2.6, eigenvalues of $-P - P^{\mathsf{T}}$ must be nonnegative. This completes our proof.

Lemma 2.10: We have

$$Q < I$$
.

Proof: According to Lemma 2.9, we have

$$\tau_j (P + P^{\mathsf{T}}) \leq O$$
,

where $\tau_i \in \mathbb{R}^+$. Further, we observe that

$$\begin{split} \frac{\tau_j}{2}P + \frac{\tau_j}{2}P^\mathsf{T} &\leq -\frac{\tau_j}{2}P - \frac{\tau_j}{2}P^\mathsf{T}, \\ I + \frac{\tau_j}{2}P + \frac{\tau_j}{2}P^\mathsf{T} + \frac{\tau_j^2}{4}PP^\mathsf{T} &\leq I - \frac{\tau_j}{2}P - \frac{\tau_j}{2}P^\mathsf{T} + \frac{\tau_j^2}{4}PP^\mathsf{T}, \\ \left(I + \frac{\tau_j}{2}P\right)\left(I + \frac{\tau_j}{2}P^\mathsf{T}\right) &\leq \left(I - \frac{\tau_j}{2}P\right)\left(I - \frac{\tau_j}{2}P^\mathsf{T}\right). \end{split}$$

The above indicates that

$$Q = \left(I - \frac{\tau_j}{2}P\right)^{-1} \left(I + \frac{\tau_j}{2}P\right) \left(I + \frac{\tau_j}{2}P^{\mathsf{T}}\right) \left(I - \frac{\tau_j}{2}P^{\mathsf{T}}\right)^{-1} \le I \tag{17}$$

due to Lemma 2.2.

We may now state

Theorem 2.11: Let $\tau_i \in \mathbb{R}^+$. We have

$$\left\|\left(I-\frac{\tau_j}{2}P\right)^{-1}\left(I+\frac{\tau_j}{2}P\right)\right\|\leq 1.$$

Proof: Firstly, recall (17) and Lemma 2.3. We may claim that

$$\left\| \left(I - \frac{\tau_j}{2} P \right)^{-1} \left(I + \frac{\tau_j}{2} P \right) \left(I + \frac{\tau_j}{2} P^\mathsf{T} \right) \left(I - \frac{\tau_j}{2} P^\mathsf{T} \right)^{-1} \right\| \leq 1.$$

Secondly, it is readily seen that

$$\left\| \left(I - \frac{\tau_j}{2} P \right)^{-1} \left(I + \frac{\tau_j}{2} P \right) \right\|^2 = \left\| \left(I - \frac{\tau_j}{2} P \right)^{-1} \left(I + \frac{\tau_j}{2} P \right) \left(I + \frac{\tau_j}{2} P \right)^{\mathsf{T}} \left(\left(I - \frac{\tau_j}{2} P \right)^{-1} \right)^{\mathsf{T}} \right\|$$

$$= \left\| \left(I - \frac{\tau_j}{2} P \right)^{-1} \left(I + \frac{\tau_j}{2} P \right) \left(I + \frac{\tau_j}{2} P^{\mathsf{T}} \right) \left(I - \frac{\tau_j}{2} P^{\mathsf{T}} \right)^{-1} \right\| \leq 1.$$

This completes our proof.

Switching our focus back to the primary concern of the stability of (14), (15). We need the following definition of what it means for a scheme to be stable.

Definition 2.12 ([8]): Let the perturbed system corresponding to a numerical method such as (14), (15) be

$$\epsilon^{(j+1)} = G\epsilon^{(j)}, \quad j = 0, 1, \dots,$$

where $\epsilon^{(j)} = q^{(j)} - \tilde{q}^{(j)}$, $\tilde{q}^{(j)}$ is a perturbed solution, and G is the perturbed coefficient matrix. We say that the numerical method is stable if there exists a uniform constant $c_0 > 0$ such that

$$||G|| \leq 1 + c_0 \tau,$$

where $\tau = \max_{0 \le \ell \le 1} \tau_{\ell} \to 0^+$ in case if nonuniform time steps [6] are considered.

Theorem 2.13: There is an accumulative error bound for the perturbed system:

$$\left\| \epsilon^{(J+1)} \right\| \leq 2c_1 \exp \left\{ \frac{-\tau_J - \tau_0 + 2T_a}{2 - \tau_0 \tilde{f}} \right\} \left\| \epsilon^{(0)} \right\|,$$

where $\tilde{f} > 0$, $c_1 > 0$, J is the last time step, and T_a is the quenching time corresponding to a > 0.

Proof: The perturbed system corresponding to (14), (15) can be written as

$$\epsilon^{(j+1)} - \frac{\tau_j}{2} \left(\psi \left(q^{(j+1)} \right) - \psi \left(\tilde{q}^{(j+1)} \right) \right) = \left(I - \frac{\tau_j}{2} P \right)^{-1} \left(I + \frac{\tau_j}{2} P \right)$$
$$\times \left[\epsilon^{(j)} + \frac{\tau_j}{2} \left(\psi \left(q^{(j)} \right) - \psi \left(\tilde{q}^{(j)} \right) \right) \right], \quad j = 0, 1, \dots, J,$$

where $q^{(j)}$, $q^{(j+1)}$ are perturbed solutions [6,12]. Traditionally the above nonlinearity must be frozen before further analysis. But here, we expand $\psi\left(q^{(\ell)}\right)-\psi\left(\tilde{q}^{(\ell)}\right)$, $\ell=j,j+1$, in a remainder form

 instead. Consequently, the above system can be converted equivalently to

$$\left(I - \frac{\tau_j}{2} F^{(j+1)}\right) \epsilon^{(j+1)} = \left(I - \frac{\tau_j}{2} P\right)^{-1} \left(I + \frac{\tau_j}{2} P\right) \left(I + \frac{\tau_j}{2} F^{(j)}\right) \epsilon^{(j)}, \quad j = 0, 1, \dots, J,$$

where $F^{(\ell)} = \psi_q\left(\hat{q}^{(\ell)}\right) \in \mathbb{R}^{N \times N}$, the vector $\hat{q}^{(\ell)}$ is between $q^{(\ell)}$, $\tilde{q}^{(\ell)}$, $\ell = j, j+1$, are diagonal Jacobi matrices involved. Note that matrices P, $F^{(\ell)}$ do not, in general, commute. Consequently,

$$\epsilon^{(j+1)} = \left(I - \frac{\tau_j}{2} F^{(j+1)}\right)^{-1} \left(I - \frac{\tau_j}{2} P\right)^{-1} \left(I + \frac{\tau_j}{2} P\right) \left(I + \frac{\tau_j}{2} F^{(j)}\right) \epsilon^{(j)} = G \epsilon^{(j)},$$

$$j = 0, 1, \dots, J.$$

It follows continuously therefore

$$\epsilon^{(j+m+1)} = \prod_{\ell=j}^{j+m} \left(I - \frac{\tau_{\ell}}{2} F^{(\ell+1)} \right)^{-1} \left(I - \frac{\tau_{\ell}}{2} P \right)^{-1} \left(I + \frac{\tau_{\ell}}{2} P \right) \left(I + \frac{\tau_{\ell}}{2} F^{(\ell)} \right) \epsilon^{(j)}$$

$$= G_{j,m} \epsilon^{(j)}, \quad j = 0, 1, \dots, J - m, \ m \ge 0.$$
(18)

We set j = 0, m = J and take a spectrum norm on both sides of (18) to yield

$$\left\| \epsilon^{(J+1)} \right\| = \left\| \prod_{\ell=0}^{J} \left(I - \frac{\tau_{\ell}}{2} F^{(\ell+1)} \right)^{-1} \left(I - \frac{\tau_{\ell}}{2} P \right)^{-1} \left(I + \frac{\tau_{\ell}}{2} P \right) \left(I + \frac{\tau_{\ell}}{2} F^{(\ell)} \right) \epsilon^{(0)} \right\|. \tag{19}$$

We may notice that both matrices $(I-\frac{\tau_\ell}{2}F^{(\ell+1)})^{-1}$ and $I+\frac{\tau_\ell}{2}F^{(\ell)}$ are diagonal since F is a diagonal matrix derived from Taylor expansions. In addition, we may choose τ_ℓ to be sufficiently small so that $0<1-\frac{\tau_\ell}{2}f_{ii}^{\ell+1}<1$. Hence the norms of these matrices remain well bounded. Let us expand the product

$$\begin{split} \epsilon^{(J+1)} &= \left(I - \frac{\tau_J}{2} F^{(J+1)}\right)^{-1} \left(I - \frac{\tau_J}{2} P\right)^{-1} \left(I + \frac{\tau_J}{2} P\right) \left(I + \frac{\tau_J}{2} F^{(J)}\right) \\ &\times \left(I - \frac{\tau_{J-1}}{2} F^{(J)}\right)^{-1} \left(I - \frac{\tau_{J-1}}{2} P\right)^{-1} \left(I + \frac{\tau_{J-1}}{2} P\right) \left(I + \frac{\tau_{J-1}}{2} F^{(J-1)}\right) \cdots \\ &\times \left(I - \frac{\tau_0}{2} F^{(1)}\right)^{-1} \left(I - \frac{\tau_0}{2} P\right)^{-1} \left(I + \frac{\tau_0}{2} P\right) \left(I + \frac{\tau_0}{2} F^{(0)}\right) \epsilon^{(0)}. \end{split}$$

Now we can add the norms back in and group certain matrices together. Denote

$$D = \left(I + \frac{\tau_J}{2} F^{(J)}\right) \left(I - \frac{\tau_{J-1}}{2} F^{(J)}\right)^{-1}.$$

Since *D* is diagonal, we have

$$||D|| = \left\| \left(I + \frac{\tau_j}{2} F^j \right) \left(I - \frac{\tau_{j-1}}{2} F^j \right)^{-1} \right\| = \max_{1 \le i \le N} \frac{1 + \frac{\tau_j}{2} f_{i,i}^j}{1 - \frac{\tau_{j-1}}{2} f_{i,i}^j}.$$

It can be observed that

$$\frac{1+\frac{\tau_{j}}{2}f_{i,i}^{j}}{1-\frac{\tau_{j-1}}{2}f_{i,i}^{j}}=1+\frac{\frac{\tau_{j-1}}{2}f_{i,i}^{j}+\frac{\tau_{j}}{2}f_{i,i}^{j}}{1-\frac{\tau_{j-1}}{2}f_{i,i}^{j}}=1+\frac{\frac{\tau_{j-1}+\tau_{j}}{2}f_{i,i}^{j}}{1-\frac{\tau_{j-1}}{2}f_{i,i}^{j}}=1+\xi \leq 1+\xi+\frac{\xi^{2}}{2!}+\frac{\xi^{3}}{3!}+\cdots=e^{\xi}.$$

Therefore

$$\|D\| \leq \max_{1 \leq i \leq N} \exp \left(\frac{\frac{\tau_{j-1} + \tau_j}{2} f_{i,i}^j}{1 - \frac{\tau_{j-1}}{2} f_{i,i}^j} \right).$$

We can implement the above on (19) and Theorem 2.9 to obtain that

$$\begin{split} \left\| \epsilon^{(J+1)} \right\| & \leq \left\| \left(I - \frac{\tau_J}{2} F^{(J+1)} \right)^{-1} \right\| \\ & \times \max_{1 \leq i \leq N} \left\{ \exp \left(\frac{(\tau_{J-1} + \tau_J) f_{i,i}^J}{2 - \tau_{J-1} f_{i,i}^J} \right) \exp \left(\frac{(\tau_{J-2} + \tau_{J-1}) f_{i,i}^{J-1}}{2 - \tau_{J-2} f_{i,i}^{J-1}} \right) \cdots \exp \left(\frac{(\tau_0 + \tau_1) f_{i,i}^1}{2 - \tau_0 f_{i,i}^1} \right) \right\} \\ & \times \left\| I + \frac{\tau_0}{2} F^{(0)} \right\| \left\| \epsilon^{(0)} \right\|. \end{split}$$

Note that if $0 < x \le y$ then $\frac{1}{-x} \le \frac{1}{-y}$. Therefore we can find the largest $f_{i,i}^J$ and denote it as \tilde{f} , and as stated earlier τ_0 is the largest time step. Hence, we acquire a new upper bound

$$\begin{split} & \left\| \left(I - \frac{\tau_{J}}{2} F^{(J+1)} \right)^{-1} \right\| \exp \left(\frac{(\tau_{J-1} + \tau_{J})\tilde{f}}{2 - \tau_{0}\tilde{f}} \right) \exp \left(\frac{(\tau_{J-2} + \tau_{J-1})\tilde{f}}{2 - \tau_{0}\tilde{f}} \right) \cdots \exp \left(\frac{(\tau_{0} + \tau_{1})\tilde{f}}{2 - \tau_{0}\tilde{f}} \right) \\ & \times \left\| \left(I + \frac{\tau_{0}}{2} F^{(0)} \right) \right\| \\ & = \left\| \left(I - \frac{\tau_{J}}{2} F^{(J+1)} \right)^{-1} \right\| \exp \left(\frac{-\tau_{J} - \tau_{0} + \sum_{i=0}^{J} 2\tau_{i}}{2 - \tau_{0}\tilde{f}} \right) \left\| I + \frac{\tau_{0}}{2} F^{(0)} \right\| \\ & = \left\| \left(I - \frac{\tau_{J}}{2} F^{(J+1)} \right)^{-1} \right\| \exp \left(\frac{-\tau_{J} - \tau_{0} + 2T_{a}}{2 - \tau_{0}\tilde{f}} \right) \left\| I + \frac{\tau_{0}}{2} F^{(0)} \right\| . \end{split}$$

Since $\tau_{\ell} \ll 1$ can be chosen small enough such that the entries of $I - \frac{\tau_{I}}{2} F^{(I+1)}$ are positive, therefore both norms above are bounded by constants. The final inequality is

$$\left\|\epsilon^{(J+1)}\right\| \leq 2c_1 \exp\left(\frac{-\tau_J - \tau_0 + 2T_a}{2 - \tau_0 \tilde{f}}\right) \left\|\epsilon^{(0)}\right\|,$$

where $c_1 = \max\left\{\left\|\left(I - \frac{\tau_J}{2}F^{(J+1)}\right)^{-1}\right\|, \left\|I + \frac{\tau_0}{2}F^{(0)}\right\|\right\}$. With this final inequality even if J goes to the infinity the error remains bounded by a uniform constant. This completes the proof.

Remark 2.1: If the nonlinear term was frozen then the diagonal matrices F would not exist. Then when applying a norm to the Pade approximation matrices, $\left(I - \frac{\tau_{\ell}}{2}P\right)^{-1} \left(I + \frac{\tau_{\ell}}{2}P\right)$, the norm is bounded by one. From there we may expect that $\epsilon^{(J+1)} < \epsilon^{(0)}$.

Remark 2.2: The proof for Theorem 2.13 depends heavily on $\psi_q(q) = (\phi(q)/d(s))$. Note $\phi(q)$ is chosen specifically to capture the dynamics of the blow-up profile. The degeneracy function, d(s), models asymptotically the defects of a thermal engine. The proof for Theorem 2.13 depends heavily on $\psi_q(q) = (\phi(q)/d(s))$. Note $\phi(q)$ is chosen specifically to capture the dynamics of the blow-up profile. The degeneracy function, d(s), models asymptotically the defects of a thermal engine.

3. Positivity, monotonicity and convergence

There are certain important multi-physical features that the finite difference approximation needs to preserve. These include the solution's positivity and monotonicity. Further, due to the strong nonlinearity involved, the commonly used Lax equivalence theorem does not hold for approximating quenching solutions [1,6,12,15]. Let \vee be one of the conventional operations <, \leq , >, \geq within this section. In particular, for $\alpha, \beta \in \mathbb{R}^N$, we assume the following operations.

- (1) $\alpha \vee \beta$ means $\alpha_k \vee \beta_k$, k = 1, 2, ..., N;
- (2) $c \vee \alpha$ means $c \vee \alpha_k$, k = 1, 2, ..., N, for any $c \in \mathbb{R}$.

In this section, when discussing if a matrix is positive or negative, it is referring to its entries. Meaning if a matrix L is positive then $l_{i,j} > 0$.

Lemma 3.1: If $\frac{\tau_j}{h_{\min}^2} < \frac{a^2 d_{\min}}{2}$, $j \in \mathbb{N}$, then matrices $I - \frac{\tau_j}{2}P$, $I + \frac{\tau_j}{2}P$ are nonsingular. Furthermore, $I + \frac{\tau_j}{2}P$ is nonnegative, $I - \frac{\tau_j}{2}P$ is monotone and inverse-positive.

Proof: Notice that

Find the specific that
$$I - \frac{\tau_j}{2}P = \operatorname{tridiag}\left(-\frac{\tau_j}{h_i(h_i + h_{i+1})d_i}, 1 + \frac{\tau_j}{h_{i+1}h_id_i}, -\frac{\tau_j}{h_{i+1}(h_i + h_{i+1})d_i}\right)$$

$$= \frac{1}{a^2}\begin{bmatrix} 1 + \frac{\tau_j}{h_1h_0d_1} & \frac{-\tau_j}{h_1(h_0 + h_1)d_1} & -\tau_j\\ \frac{-\tau_j}{h_1(h_1 + h_2)d_2} & 1 + \frac{\tau_j}{h_2h_1d_2} & \frac{-\tau_j}{h_2(h_1 + h_2)d_2}\\ & \cdots & -\tau_j\\ \frac{-\tau_j}{h_{n-2}(h_{n-2} + h_{n-1})d_{n-1}} \end{bmatrix}$$

$$\frac{1 + \frac{\tau_j}{h_{n-1}h_{n-2}d_{n-1}}}{\frac{-\tau_j}{h_{n-1}(h_{n-1} + h_n)d_n}} \quad \frac{-\tau_j}{h_{n-1}(h_{n-2} + h_{n-1})d_{n-1}} \\ \frac{1 + \frac{\tau_j}{h_{n-1}(h_{n-1} + h_n)d_n}}{1 + \frac{\tau_j}{h_nh_{n-1}d_n}} \right].$$

To prove that $I - \frac{\tau_j}{2}P$ is nonsingular we only need to show that zero is not an eigenvalue. Let us find the location of the eigenvalues using Lemma 2.8. To clarify Lemma 2.8 will tell us the circles in which the eigenvalues are contained. Since the diagonal entries of the matrix $I - \frac{\tau_j}{2}P$ are positive then the centre of the Gershgorin circles will be away from zero. Let us show the radius of the circles is small enough such that the zero is never in the circles. To this end, we notice that

$$\begin{split} 1 + \frac{\tau_j}{h_1 h_0 d_1} + \frac{-\tau_j}{h_1 (h_0 + h_1) d_1} &= 1 + \frac{\tau_j}{d_1} \left(\frac{h_0 + h_1}{h_1 h_0 (h_0 + h_1)} - \frac{h_0}{h_1 h_0 (h_0 + h_1)} \right) \\ &= 1 + \frac{\tau_j}{h_0 (h_0 + h_1) d_1}. \end{split}$$

Since τ_i , d_1 and the steps are positive then the above summation is greater than the unity. The same algebra can be applied to the last row of the matrix. Now let us see what may happen with the rest of the rows of $I - \frac{\tau_j}{2}P$. Without loss of generality let us focus on the summation of the second row. Notice

$$-\frac{\tau_j}{h_1(h_1+h_2)d_2} + 1 + \frac{\tau_j}{h_2h_1d_2} - \frac{\tau_j}{h_2(h_1+h_2)d_2}$$

$$= 1 + \frac{\tau_j}{d_2} \left(-\frac{h_2}{h_2h_1(h_1+h_2)} + \frac{h_1+h_2}{h_2h_1(h_1+h_2)} - \frac{h_1}{h_2h_1(h_1+h_2)} \right) = 1.$$

Therefore based on the Gershgorin Circle Criterion it is clear that the eigenvalues of $I - \frac{\tau_j}{2}P$ cannot be 0. Therefore $I - \frac{\tau_j}{2}P$ is nonsingular.

On the other hand, the matrix $I + \frac{\tau_j}{2}P$ has a similar structure,

$$I + \frac{\tau_{j}}{2}P$$

$$= \frac{1}{a^{2}} \begin{bmatrix} 1 - \frac{\tau_{j}}{h_{1}h_{0}d_{1}} & \frac{\tau_{j}}{h_{1}(h_{0} + h_{1})d_{1}} & \frac{\tau_{j}}{h_{2}(h_{1} + h_{2})d_{2}} \\ \frac{1}{h_{1}(h_{1} + h_{2})d_{2}} & \frac{\tau_{j}}{h_{2}h_{1}d_{2}} & \frac{\tau_{j}}{h_{2}(h_{1} + h_{2})d_{2}} \\ & \ddots & & \\ & & \frac{\tau_{j}}{h_{n-2}(h_{n-2} + h_{n-1})d_{n-1}} \end{bmatrix}$$

$$1 - \frac{\tau_{j}}{h_{n-1}h_{n-2}d_{n-1}} & \frac{\tau_{j}}{h_{n-1}(h_{n-2} + h_{n-1})d_{n-1}} \\ \frac{1}{h_{n-1}(h_{n-1} + h_{n})d_{n}} & 1 - \frac{\tau_{j}}{h_{n}h_{n-1}d_{n}} \end{bmatrix}$$

By the same token, we may show that the real part of the eigenvalues of the above matrix is bounded above by 1 and below by $1-\frac{2\tau_j}{a^2h_{\min}^2d_{\min}}$. Recall by the assumptions $\frac{\tau_j}{h_{\min}^2}<\frac{a^2d_{\min}}{2},\ j\in\mathbb{N}$. Therefore the eigenvalues are bounded below by zero and $I + \frac{\tau_j}{2}P$ is nonsingular. By $I + \frac{\tau_j}{2}P$ structure and our assumptions, it is clear the matrix's entries are nonnegative. All there is to show is that $I - \frac{\tau_j}{2}P$ is monotone and inverse-positive. To do this we need to define a couple of things. Notice matrix $I - \frac{\tau_j}{2}P$ is a Z-Matrix because of its structure. Furthermore, $I - \frac{\tau_j}{2}P$ the real part of the eigenvalues is greater than or equal to one hence $I - \frac{\tau_j}{2}P$ is an M-Matrix. By Lemma 2.7 matrix $I - \frac{\tau_j}{2}P$ is monotone and has an inverse-positive.

Lemma 3.2: If $\frac{\tau_j}{h_{\min}^2} < \frac{a^2 d_{\min}}{2}$, $j \in \mathbb{N}$, and $\frac{\tau_j \psi_q(\xi_k^{(j)})}{2} < 1$, k = 1, 2, ..., N, $j = 0, 1, ..., \ell$, $q^{(j)} \le \xi^{(j)} \le 1$ $q^{(j+1)}$, then our nonuniform finite difference approximation, which is derived from Equations (14) to (15), is positive, that is, $q^{(j)} > 0$ for all valid indexes j

Proof: Let us use an induction to prove this. First of all, we show the base case. Notice that

$$q^{(1)} = \left(I - \frac{\tau_0}{2}P\right)^{-1} \left(I + \frac{\tau_0}{2}P\right) \left[q^{(0)} + \frac{\tau_0}{2}\psi\left(q^{(0)}\right)\right] + \frac{\tau_0}{2}\psi\left(q^{(1)}\right).$$

Utilizing a Taylor expansion of $\psi(q^{(1)})$ at the zero vector 0, we observe that $\psi(q^{(1)}) = \psi(0) +$ $\psi_q(\xi^{(1)})(q^{(1)}-0)$, where $\xi^{(1)}$ is within the span of 0 and $q^{(1)}$. We further notice that $\psi(0)=$

 $(\psi_1(0), \psi_2(0), \dots, \psi_N(0)) = ((1-0)^r/d_1, (1-0)^r/d_2, \dots (1-0)^r/d_N) = (1/d_1, 1/d_2, \dots 1/d_N).$ Therefore

$$q^{(1)} = \left(I - \frac{\tau_0}{2} \psi_q(\xi^{(1)})\right)^{-1} \left[\left(I - \frac{\tau_0}{2} P\right)^{-1} \left(I + \frac{\tau_0}{2} P\right) \left[q^{(0)} + \frac{\tau_0}{2} \psi\left(q^{(0)}\right) \right] + \psi(0) \right].$$

Recall Lemma 3.1 that $I + \frac{\tau_0}{2}P$ is nonnegative for sufficiently small time steps τ_j , and $I - \frac{\tau_0}{2}P$ is inversely positive. Also the function ψ is increasing. Note that $\psi(0)$ depends entirely on the degenerate function $a\alpha s^{\theta}(1-s)^{1-\theta}$. Since the variable s has the range 0 < s < 1, then the vector $\psi(0)$ is positive. Now all we need for $q^{(1)}$ to be positive is that $q^{(0)}$ is positive. But the initial value $q^{(0)}$ is positive by definition. Thus we are done with the base case. Secondly, we assume that $q^{(j)} > 0$ and all there is left for us to show is $q^{(j+1)} > 0$. Just as in the base case, let us expand $q^{(j+1)}$ with our method

$$q^{(j+1)} = \left(I - \frac{\tau_j}{2} \psi_q(\xi^{(j+1)})\right)^{-1} \left[\left(I - \frac{\tau_j}{2} P\right)^{-1} \left(I + \frac{\tau_j}{2} P\right) \left[q^{(j)} + \frac{\tau_j}{2} \psi\left(q^{(j)}\right)\right] + \psi(0)\right].$$

By the assumption $q^{(j)} > 0$ and $\psi(q)$ is monotonically increasing, therefore $q^{(j+1)} > 0$.

Remark 3.1: If the nonlinear term involved was frozen then there would not be a need for $\frac{\tau_j \psi_q(\xi_k^{(j)})}{2}$ < 1, k = 1, 2, ..., N, $j = 0, 1, ..., \ell$. Therefore the proof can be implemented differently, for instance, see discussions offered in [20].

Theorem 3.3: Let $\tau_i \phi_{\text{max}} < 1$, $j \in \mathbb{N}$. If there exits $\ell > 0$ such that

- (i) $\frac{\tau_j}{h_{\min}^2} < \frac{a^2 d_{\min}}{2}, j = 0, 1, \dots, \ell$
- (ii) $\tau_j Pq^{(j)} + \tau_j \psi(q^{(j)}) \ge 0, j = 0, 1, \dots, \ell,$
- (iii) $\frac{\tau_j \psi_q(\xi_k^{(j)})}{2} < 1, k = 1, 2, ..., N, j = 0, 1, ..., \ell$

then the partial solution sequence, $q^{(0)}, q^{(1)}, \ldots, q^{(\ell)}$ generated by the nonuniform method (14), (15) is monotonically increasing.

Proof: Similar to the proof of Theorem 2.8, we may commence with an expansion of $q^{(j+1)}$, that is,

$$\begin{split} q^{(j+1)} &= q^{(j)} = \left(I - \frac{\tau_{j}}{2}P\right)^{-1} \left(I + \frac{\tau_{j}}{2}P\right) \left(q^{(j)} + \frac{\tau_{j}}{2}\psi\left(q^{(j)}\right)\right) + \frac{\tau_{j}}{2}\psi\left(q^{(j+1)}\right) - q^{(j)} \\ &= \left(I - \frac{\tau_{j}}{2}P\right)^{-1} \left[\left(I + \frac{\tau_{j}}{2}P\right) \left(q^{(j)} + \frac{\tau_{j}}{2}\psi\left(q^{(j)}\right)\right) + \left(I - \frac{\tau_{j}}{2}P\right) \left(\frac{\tau_{j}}{2}\psi\left(q^{(j+1)}\right) - q^{(j)}\right)\right] \\ &= \left(I - \frac{\tau_{j}}{2}P\right)^{-1} \left[\tau_{j}Pq^{(j)} + \left(I + \frac{\tau_{j}}{2}P\right) \left(\frac{\tau_{j}}{2}\psi\left(q^{(j)}\right)\right) + \left(I - \frac{\tau_{j}}{2}P\right) \left(\frac{\tau_{j}}{2}\psi\left(q^{(j+1)}\right)\right)\right] \end{split}$$

Implementing Taylor expansion on $\psi\left(q^{(j+1)}\right)$ at $q^{(j)}$, we will get $\psi\left(q^{j}\right)+\psi_{q}(\xi^{(1)})\left(q^{(j+1)}-q^{(j)}\right)$. Therefore we get

$$= \left(I - \frac{\tau_{j}}{2}P\right)^{-1} \left[\tau_{j}Pq^{(j)} + \left(I + \frac{\tau_{j}}{2}P\right)\left(\frac{\tau_{j}}{2}\psi(q^{(j)})\right) + \left(I - \frac{\tau_{j}}{2}P\right)\frac{\tau_{j}}{2}\left(\psi\left(q^{j}\right) + \psi_{q}(\xi^{(1)})\left(q^{(j+1)} - q^{(j)}\right)\right)\right]$$

$$= \left(I - \frac{\tau_{j}}{2}P\right)^{-1} \left[\tau_{j}Pq^{(j)} + \tau_{j}\psi(q^{(j)}) + \left(I - \frac{\tau_{j}}{2}P\right)\left(\psi_{q}(\xi^{(1)})\left(q^{(j+1)} - q^{(j)}\right)\right)\right].$$

Finally, combine everything to get

613

614

615 616 617

618

619

620 621 622

623

624 625

626

627 628

629

630

631

632

633

634 635

636

637

638

639

640

641

642

643

644

645

646

647

648

649

650 651

652

653 654 655

656

657

658

659

660 661

662

663

$$q^{(j+1)} - q^{(j)} = \left(I - \frac{\tau_j}{2} \psi_q(\xi^{(1)})\right)^{-1} \left(I - \frac{\tau_j}{2} P\right)^{-1} \tau_j \left[Pq^{(j)} + \psi\left(q^j\right)\right]$$

By lemma 3.2 $\left(I - \frac{\tau_j}{2}P\right)^{-1}$ has positive entries and by the assumptions $\tau_j Pq^{(j)} + \tau_j \psi(q^{(j)})$ is a positive vector. All that is needed for the solution to be monotonic increasing is to make τ_i small enough so that $\left(I - \frac{\tau_j}{2} \psi_q(\xi^{(1)})\right) > 0$. This completes the proof.

Remark 3.2: Fewer hypotheses are needed for Theorem 3.3 if, again, the nonlinear term involved is frozen.

4. Simulation experiments and order estimates

Let $r \equiv 1$ in (4). Without loss of generality, we consider the numerical solution of the following standardized degenerate modelling problem throughout our experiments.

$$a\alpha s^{\theta} (1-s)^{1-\theta} \frac{\partial q}{\partial t} = \frac{1}{a^2} \frac{\partial^2 q}{\partial s^2} + \frac{1}{1-q}, \quad 0 < s < 1, \ t_0 < t \le T_a, \ a \ge a^* > 1,$$
 (20)

$$q(0,t) = q(1,t) = 0, \quad t > t_0,$$
 (21)

$$q(s, t_0) = q_0(s), \quad 0 \le s \le 1,$$
 (22)

where $0 \le \theta \le 1$ is the degeneracy indicator, and a^* is the critical length [2,9,14,18]. For the purpose of comparisons with existing results, we are particularly interested in the case of $q_0(s)$ $0.01\sin(\pi s),\ 0 \le s \le 1,\ a = \pi, \alpha = 1,\ \text{and}\ t_0 = 0.$ Traditionally, a spacial mesh for quenching solution computations is uniform which results in inaccurate numerical solutions if the uniform mesh step, h, used is too large, especially immediately before quenching [11,19]. On the other hand, if h is chosen to be too small, the overall efficiency of the finite difference algorithm may decline dramatically and additional computational errors may be accumulated earlier.

Indeed, arc-length adaptations can be employed effectively throughout quenching solution calculations. However the procedure is relatively complicated and evaluations of nonlinear systems of equations are often necessary to readjust mesh steps [2,6,11].

Since solutions of problems such as (5)–(7) and (20)–(22) are known for a single hot point throughout the fuel combustion and a single point quenching/ignition is expected [5,14,16], in continuing investigations, we shall introduce a new moving mesh adaptation as the Quenching Seeking Moving Mesh Method (QSM³) without calculating traditional arc-lengths. This straightforward procedure consists of the following steps.

- Choose the most favourable spacial mesh distribution for approximating the underlying quenching singularity of q or q_t . The single point quenching location is assumed to be at s_k^* .
- (2) Choose a sequence $\{k_\ell\}_{k=1}^M$, $k_\ell \in \mathbb{N}^+$, $k_1 < k_2 < \cdots k_M < K$, where K is the maximal number of temporal steps expected.
- (3) Locate the maximal component of q^{k_ℓ} , or $q_t^{k_\ell}$, at each temporal level of k_ℓ , $1 \le \ell \le M$. Denote this position as $s_{k_{\ell}}^*$.
- (4) Replace the previous location $s_{k_{\ell-1}}^*$ by $s_{k_{\ell}}^*$. Shift the nonuniform spacial mesh accordingly. Use it to compute further numerical solutions q^k , $k = k_\ell + 1, k_\ell + 2, \dots, k_{\ell+1} \le K$.
- (5) Repeat steps 3, 4 till the maximal number of steps *K* is reached.

Needless to say, gaps between $k_{\ell}, k_{\ell+1}$ are not necessary constants, though the simplest choice is to assume that $k_{\ell} = k_{\ell-1} + 1$, $\ell = 1, 2, \dots, M$. As usual, cubic splines may be chosen to transfer data

666 667

668

669

670

671 672

673

674 675

676

677

678

679

680

681

682

683

684

685

686

687

688

689

690

691

692

693

694

695

696

697

698

699

700

701

702

703

704

705

706

707 708

709

710 711

712 713

714

between levels k_ℓ and $k_\ell+1$. We anticipate that $\{s_{k_\ell}\}_{k=1}^M \to s^*$ as $M\to\infty$ at quenching. Merits of the QSM^3 are threefold.

- The distribution of nonuniform mesh is predetermined. This simplifies the adaptive procedure since traditional arc-length calculations are completely avoided.
- To search for a maximal element in a solution vector is extremely robotic and straightforward. The procedure effectively improves the efficiency of computations. This will also be confirmed in our
- The choice of $\{k_\ell\}_{\ell=1}^M$ is flexible and in most cases, we do not need to start a maximal value search until close to the quenching.

The following experiments will demonstrate how the change in the degeneracy function or more specifically θ will affect the quenching location. Note that θ is stochastic in our Bernoulli type degenerate function d (20). Thus we only need to show the degeneracy effects by choosing several special θ values as illustrations. To this end, without loss of generality, we take the Fibonacci number $\theta_1 = 2/(1+\sqrt{5}) \approx 0.61803398$, and the corresponding inverse Fibonacci number in experiments. Note that values of the parameter do not contribute to the quenching time, but affect the quenching location [18,20]. To reiterate $a = \pi$. In our experiments, it is observed that the quenching time $T_a \approx 0.78735$ and $s^* \approx 0.41156211$. Figure 1 gives surface plots of the solution q and its temporal derivative q_t at quenching time. The top row corresponds to $\theta_1 = 2/(1+\sqrt{5})$, and notice both the solution and its derivative are non-symmetric. The second experiment is kept the same with the change of θ . This time we take $\theta_2 = 1 - 2/(1 + \sqrt{5}) \approx 0.38196601$. The bottom row of Figure 1 shows that the solution now shifts to the right closer to s = 1 instead of the left like before. The reason for this phenomenon is that our degeneracy function $s^{\theta}(1-s)^{1-\theta}$ depends on the indicator index θ proportionally.

For the experiments, the nonlinear distribution of mesh steps is created based on the exponential Gauss error function [22], and the minimum h location is chosen at s = 0.5 for simplicity. As numerical experiments continue toward the quenching location, it becomes clear that the location of minimal h is shifted robotically following the movement of the maximum of q. In Figure 3, we show the trajectories of the functions $\max_{0 \le s \le 1} q(x,t)$ and $\sup_{0 < s < 1} q_t(x,t)$ for time t close to the quenching time $T_a \approx 0.78735$. We utilize the degeneracy index $\theta_1 = 2/(1+\sqrt{5})$ in the experiment since results based on other index values are similar. The positivity and monotonicity of the functions are visible. Following either trajectory, we may implement a particular QSM³ procedure. Further, in Figure 2, for $\theta_1 = 2/(1+\sqrt{5})$ we have the minimal h location $s_{k\ell}^* \approx 0.30707558$ at t = 0.4. Then the location gradually converges to the quenching location $s^* \approx 0.41156211$. In the second case with $\theta_2 = 1 - 2/(1 + \sqrt{5})$, we have $s_{k_\ell}^* = 0.69956416$ at t = 0.4. The location shifts then smoothly to its final location $s^* = 0.5851847$. The profiles are utilized precisely by our QSM³ procedures.

In continuing explorations, we wish to examine the order of convergence of the finite difference method (14), (15). We only need to consider the order in space since the convergence order in time can be estimated through Courant constraints [4,21]. To this end, we utilize a generalized pointwise Milne device and define

$$p = \frac{1}{\ln(1/2)} \ln \left(\frac{|q_{h/4}^{\tau} - q_{h/2}^{\tau}|}{|q_{h/2}^{\tau} - q_{h}^{\tau}|} \right), \tag{23}$$

where $q_h^{ au}$ is the solution computed on time step au and spatial step h, $q_{h/2}^{ au}$ is the solution on steps auand h/2, and similarly, $q_{h/4}^{\tau}$ is on τ and h/4 [12,15].

A key point of Figure 4. is that the final order of convergence significantly decreases at the quenching locations (the location depends on the index value of θ used). However, the reduced orders of convergence in both θ_1, θ_2 cases are still greater than p = 1.95 which is evident that the overall order of convergence of the nonuniform finite difference method (14), (15) is approximately quadratic.

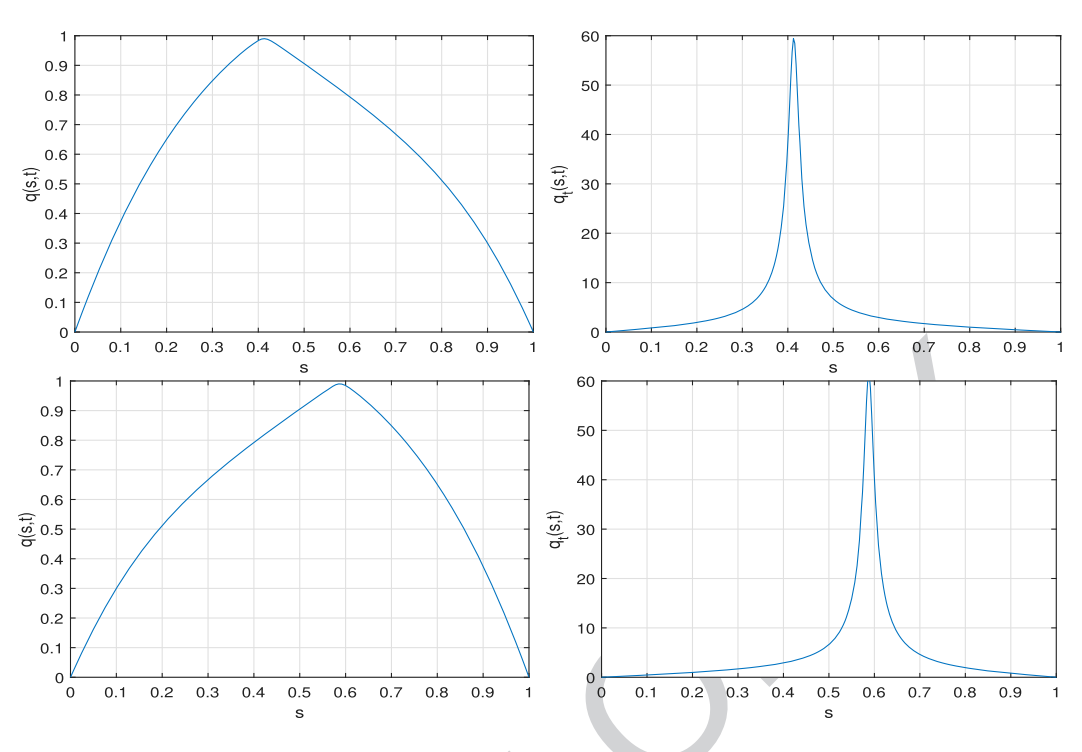


Figure 1. While graphs on the left are for the solution q, graphs on the right are for the derivative function q_t , both corresponding to two different values of θ , respectively, and immediately before quenching. The quenching time observed, $T_a \approx 0.78735$, is highly consistent with existing results [18,20,23]. QSM³ is used.

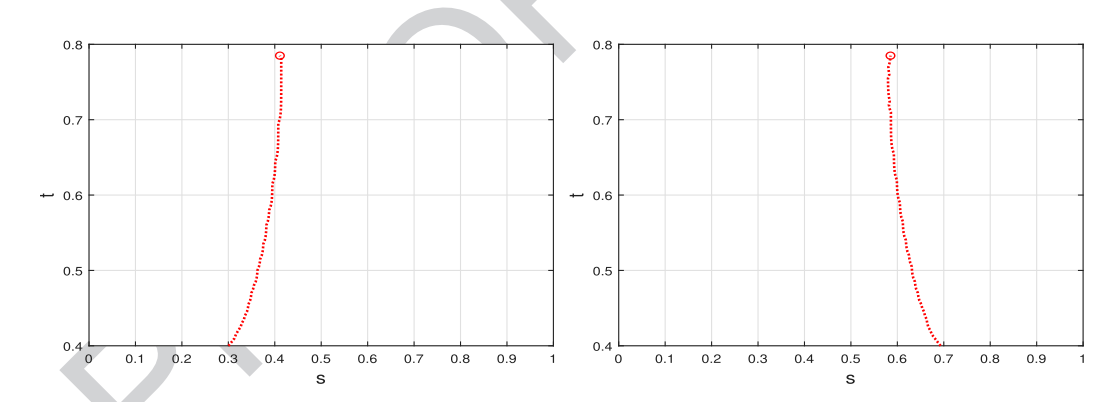
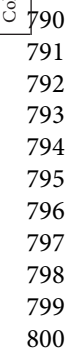


Figure 2. The left figure shows the trajectory of $s_{k_{\ell}}^*$ corresponding to θ_1 . The right figure shows the trajectory of $s_{k_{\ell}}^*$ corresponding to θ_2 . Both trajectories match precisely profiles of the quenching solutions shown in Figure 1.

In Table 1, we list experimental values of maximal, minimal, mean value, and median of the pointwise orders of convergence of the numerical method (14) and (15). The two typical degeneracy indexes are employed. It is justified to conclude that the order of the convergence in space is approximately two, though the order of convergence surfaces are clearly nonlinear. We may recall that the location of quenching is $s^* \approx 0.41156211$ for θ_1 and $s^* \approx 0.58843788$ for θ_2 , respectively.

Figure 5 is devoted to the final distribution of the variable spacial mesh points. A total number of mesh points N = 202 is utilized in both cases associated with θ_1, θ_2 . We note that, even though the minimal location of the distribution is at s = 0.5 at t = 0, the distribution of variable mesh points



10² max(q) and sup(q,) 10¹ 10⁰ 0.4 0.5 0.6 0.7 0.8

Figure 3. The trajectories of the functions $\max_{0 \le s \le 1} q(x,t)$ (black curve) and $\sup_{0 < s < 1} q_t(x,t)$ (red curve) for $t \in [0.37, T_a]$ are shown in a *y*-logarithmic scale for better clarity. The simulation is based on the index value θ_1 . Clearly, the two functions are nonnegative and monotonically increasing as $t \to T_a \approx 0.78735$. A QSM³ procedure is used.

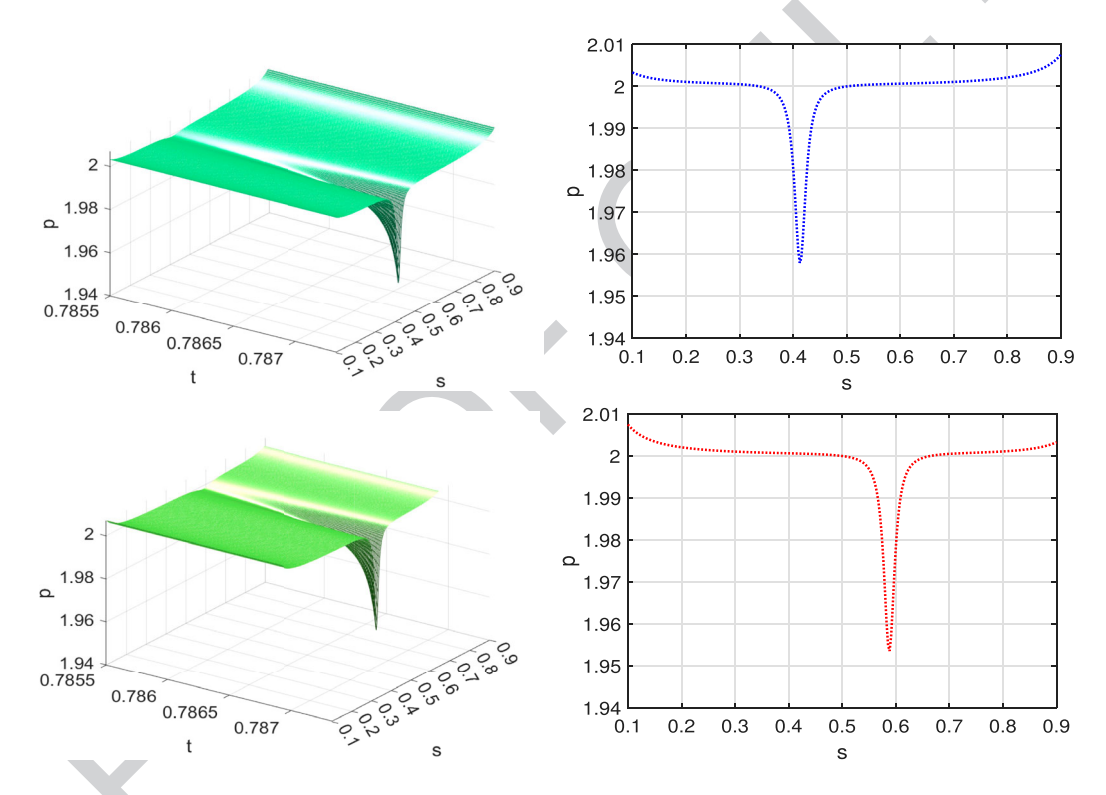


Figure 4. Figures on the left are for the pointwise order of convergence surface within a small temporal interval $t \in$ [0.78550, 0.78735] before quenching. The final order of convergence profiles prior to quenching are shown on the right. Indexes θ_1 , θ_2 are considered and $T_a \approx 0.78735$ is observed. QSM³ is used.

Table 1. Order of convergence data are taken at $T_1 = 0.78734$ and $T_2 = 0.78735$, respectively.

θ	$ heta_1 pprox$	0.61803398	$ heta_{2} pprox$	0.38196601
p	<i>T</i> ₁	T ₂	<i>T</i> ₁	T ₂
Maximum rate	2.00843233	2.00843384	2.00730427	2.00730549
Minimum rate	1.95792548	1.97167351	1.95346389	1.96937480
Mean rate	1.99840645	1.99900013	1.99808714	1.99876299
Median rate	2.00066861	2.00066875	2.00061659	2.00061673

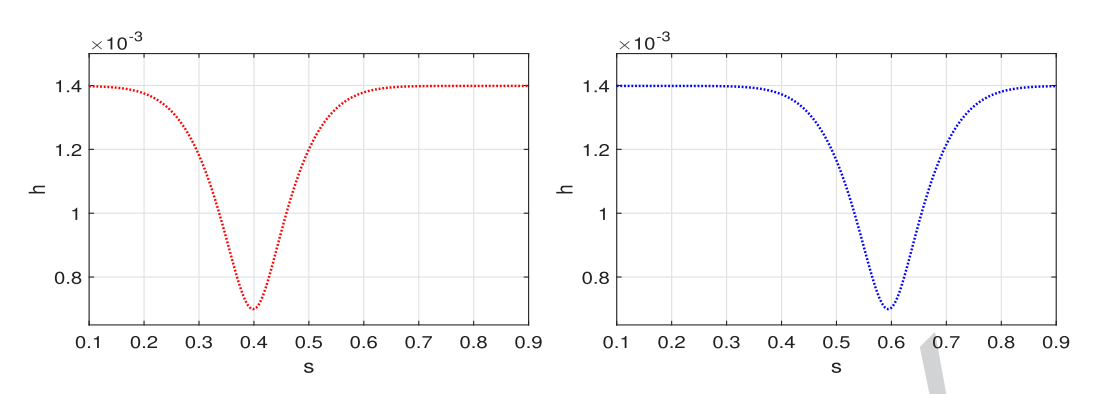


Figure 5. Terminal variable spacial step h distributions. The left figure is for the case when θ_1 is used and the right figure is for the case of θ_2 . We notice that the minimal step locations coincide with the quenching locations in two cases, respectively. A total number of N=202 mesh points are used in each case.

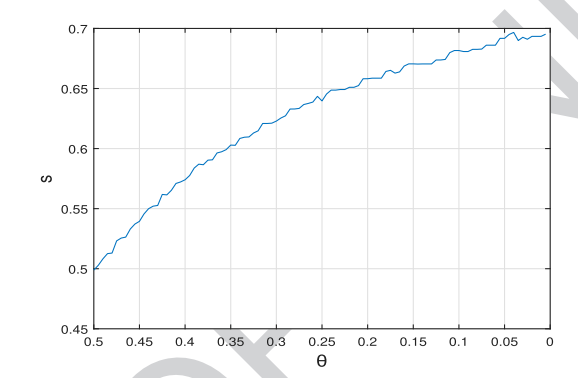


Figure 6. The decrease in θ shifts the quenching location to from 0.5 to 0.7.

evolutes to the respective quenching location robotically through our QSM³ moving mesh adaptations. This is surely evidence of the success of the straightforward method which improves both the accuracy and efficiency of the simulation method.

Note that our degenerate function d(s) defined in (1.4) is symmetric, therefore investigations of its impacts on the numerical solution only need to be carried out within $\theta \in [0, 1/2]$. While Figures 1–5 have already shown part of the impacts, the next simulation will illustrate further how much the quenching location is affected by various values of $0 \le \theta \le 1/2$. The quenching location decreases monotonically as θ increases within the interval (0.45, 0.7). The phenomenon is highly consistent with known results [15,18,20].

Further, the correlation between the change in θ and the quenching location seems to be quadratic, though more rigorous theoretical proofs need to be fulfilled.

A demonstration of how the quenching location is shifted can be seen in Figure 7. There everything is kept the same while three distinct θ 's are chosen. A similar impact on the quenching location occurs for $1/2 \le \theta \le 1$ can be observed. The quenching location seems to decrease to 0.3 as a increases.

As an extended experiment, we now consider a non-symmetric degenerate function $d(s) = a\alpha s^{\theta}(1-s)^{1-\theta}$, 0 < s < 1 where $\theta = 0.2$. In Figure 8, θ is kept constant while the interval size a changes from 3 to 53 which is intentionally beyond the critical size [5,15,20]. Unlike the previous experiment, the quenching location goes past s = 0.7 and comes close to the boundary. A possible explanation for this phenomenon is that the non-symmetric degenerate function has more weight towards s = 1 as the value of a is increased. Needless to say, a more precise analysis of such nonlinearity impacts needs to be implemented in our forthcoming studies.

\$71

\$72

\$73

\$76

Colour online, B/W in print

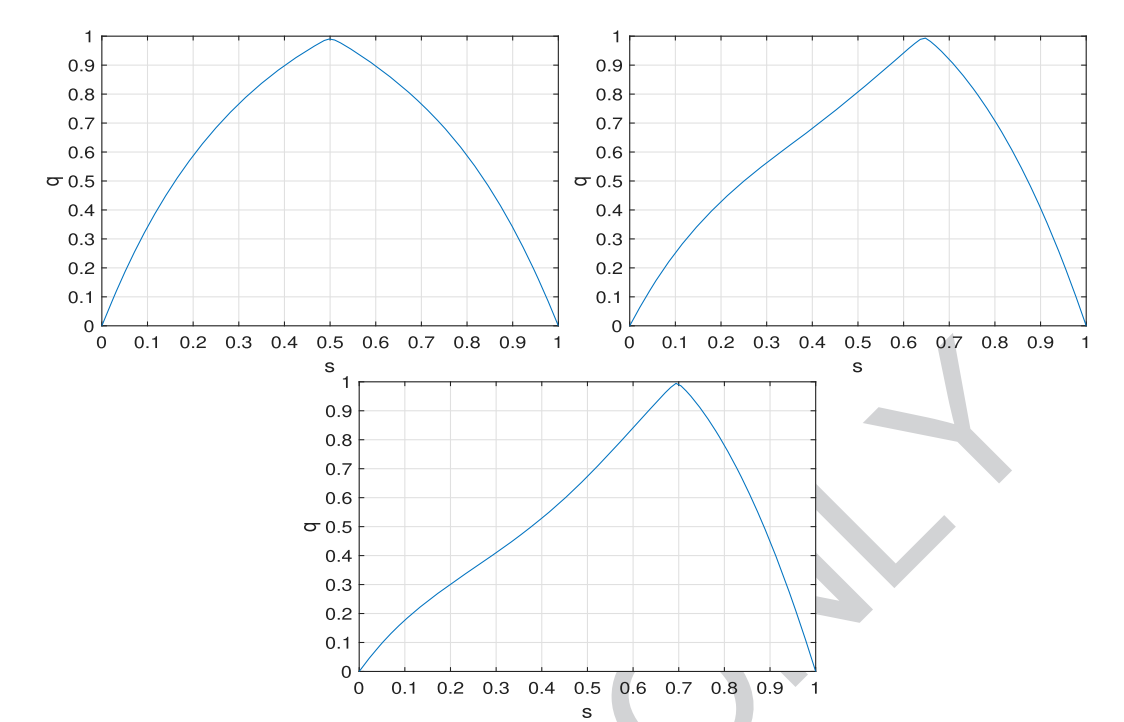


Figure 7. The relation between the degeneracy parameter θ and quenching location. The θ is 0.5 in the first graph, 0.25 in the second, and 0.01 in the third.

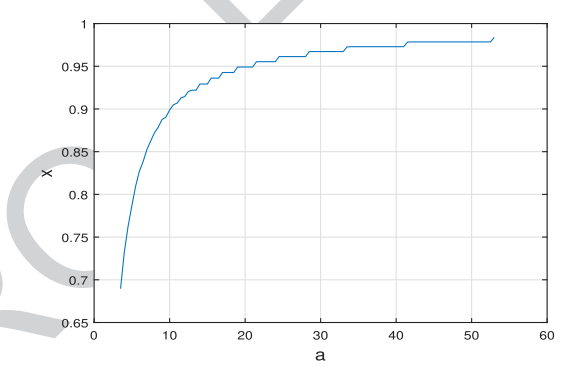


Figure 8. The simulated correlation between the interval size a and quenching location. Again, a fixed parameter $\theta=0.2$ is used.

5. Conclusions and expectations

In this paper, we have shown that the designated Crank-Nicholson method on time-space nonuniform grids is stable. The proof is accomplished without requiring the nonlinear source term to be frozen. The mathematical analysis does not rely on any traditional assumption that the coefficient matrix must be symmetric. These mean that the analysis can be extended further for solving higher-order partial differential equation problems via either finite difference or deep neural network approximations. The main driving force behind our analysis is the use of proper Padé approximants for an applicable unit bound. The nonuniform spacial mesh used is controlled through a QSM³ moving strategy which not only simplifies the nonlinear adaptation procedure but also raises the efficiency in computations. It was found that the numerical solution captures key quenching solution features such as positivity and monotonicity once necessary constraints are met. Under the same constraints, the finite difference method implemented is proved to be convergent. Simulation experiments further indicate that the spacial order of convergence is quadratic except in the neighbourhood of the quenching location as time t approaches the quenching time T_a . Our continuing explorations include extending the mathematical analysis for approximations of higher-order Kawarada problems and verifying the conservation features mentioned above more precisely. More dynamic moving mesh strategies based on the idea of QSM³ formation will also be investigated. Operator splitting and deep neural network approximations will also be introduced.

Disclosure statement

No potential conflict of interest was reported by the author(s).

Funding

Both authors would like to thank the editor and anonymous reviewers for their time spent and the invaluable comments given. The suggestions have significantly improved the quality and presentation of this paper. Both authors would also appreciate the National Science Foundation USA, and Simons Foundation USA for generous support through [grant number DMS-2318032; NSF] and [grant number MPS-1001466; SIMONS].

ORCID

Oin Sheng http://orcid.org/0000-0003-0528-8560

References

- [1] M.A. Beauregard and Q. Sheng, An adaptive splitting approach for the quenching solution of reaction-diffusion equations over nonuniform grids, J. Comp. Appl. Math. 241 (2013), pp. 30–44.
- [2] M.A. Beauregard and Q. Sheng, Explorations and expectations of equidistribution adaptations for nonlinear quenching problems, Adv. Appl. Math. Mech. 5(4) (2013), pp. 407-422.
- [3] A. Berman and R. Plemmons, Nonnegative Matrices in the Mathematical Sciences, Academic Press, Cambridge, MA, 2014.
- [4] S. Boscarino, R. Bürger, P. Mulet, G. Russo, and L.M. Villada, Linearly implicit IMEX Runge-Kutta methods for a class of degenerate convection-diffusion problems, SIAM J. Sci. Comput. 37(2) (2015), pp. B305–B331.
- [5] C.Y. Chan, A quenching criterion for a multi-dimensional parabolic problem due to a concentrated nonlinear source term, J. Comput. Appl. Math. 235(13) (2011), pp. 2734–2737.
- [6] H. Cheng, P. Lin, Q. Sheng, and R.C.E. Tan, Solving degenerate reaction-diffusion equations via variable step Peaceman-Rachford splitting, SIAM J. Sci. Comput. 25(4) (2003), pp. 1273–1292.
- [7] G.H. Golub and C.F. Van Loan, *Matrix Computations*, 4th ed., Johns Hopkins University Press, Baltimore and London, 2013.
- [8] E. Hairer and A. Iserles, *Numerical stability in the presence of variable coefficients*, Found. Comput. Math. 16 (2016), pp. 751–777.
- [9] J.K. Hale, Asymptotic Behavior of Dissipative Systems, American Math Soc, Philadelphia, PA, 1988.
- [10] R.A. Horn and C. Johnson, Matrix Analysis, 2nd ed., Cambridge University Press, Cambridge and London, 1990.
- [11] W. Huang and R.D. Russell, Adaptive Moving Mesh Methods, Springer Nature, Zürich, Switzerland, 2011.
- [12] A. Iserles, A First Course in the Numerical Analysis of Differential Equations, 2nd ed., Cambridge University Press, Cambridge and London, 2009.
- [13] H. Kawarada, On solutions of initial-boundary value problems for $u_t = u_{xx} + 1/(1-u)$, Publ. Res. Inst. Math. Sci. 10 (1975), pp. 729–736.
- [14] H.A. Levine, Quenching, nonquenching, and beyond quenching for solution of some parabolic equations, Ann. Mat. Pura Appl. 155 (1989), pp. 243–260.
- [15] J.L. Padgett and Q. Sheng, Numerical solution of degenerate stochastic Kawarada equations via a semi-discretized approach, Appl. Math. Comput. 325 (2018), pp. 210–226.
- [16] T. Poinset and D. Veynante, Theoretical and Numerical Combustion, 2nd ed., Edwards Publisher, Philadelphia, PA, 2005.
- [17] Y. Saad, Iterative Methods for Sparse Linear Systems, 2nd ed., SIAM, Philadelphia, PA, 1996.
- [18] Q. Sheng and Y. Ge, A numerical endeavor with nonlinear Kawarada equations, Dyn. Syst. Appl. 25 (2016), pp. 543–556.
- [19] Q. Sheng and A.Q.M. Khaliq, *Integral Methods in Science and Engineering (Research Notes in Math)*, Chapman and Hall/CRC, London and New York, 2001. Ch. 9. A monotonically convergent adaptive method for nonlinear combustion problems.

Q2

Q1

- [20] Q. Sheng and A.Q.M. Khaliq, A revisit of the semi-adaptive method for singular degenerate reaction-diffusion equations, East Asia J. Appl. Math. 2 (2012), pp. 185–203.
- [21] Q. Sheng and E.S. Torres, A nonconventional stability approach for a nonlinear Crank-Nicolson method solving degenerate Kawarada problems, Appl. Math. Lett. 144 (2023), pp. 108730.
- [22] E.T. Whittaker and G.N. Watson, A Course of Modern Analysis, 4th ed., Cambridge University Press, Cambridge and London, 1996.
- [23] L. Zhu, N. Liu, and Q. Sheng, A simulation expressivity of the quenching phenomenon in a two-sided space-fractional diffusion equation, Appl. Math. Comput. 437 (2023), pp. 127523.